



Geochemical, mineralogical, and microstructural characteristics of fault rocks and their impact on TBM jamming: a case study

Peng Lin^{1,3,4} · Tengfei Yu^{1,2} · Zhenhao Xu^{1,4}  · Ruiqi Shao⁴ · Wenyang Wang⁴

Received: 15 December 2020 / Accepted: 16 December 2021 / Published online: 10 January 2022
© Springer-Verlag GmbH Germany, part of Springer Nature 2022

Abstract

Faults can represent adverse geological conditions that frequently cause the jamming of tunnel boring machines (TBMs). In this study, we present a case study of TBM jamming at mileage 106+402.8 in the TBM 2 bid section of the Central Yellow River Diversion in China. Firstly, we identify possible jamming hazards. In addition, a fault between dolomitic limestone and granite was revealed by the geological investigation. Secondly, by comprehensively analyzing the geochemical, mineralogical, and microstructural characteristics of the host and fault rocks, we identify the compressional torsional fault FT₂ and the nearby fault rocks. Finally, we explore how the geological characteristics of the fault rocks affect the likelihood of TBM jamming. Our results indicate that geochemical effects and long-term tectonic stresses caused major changes in the structure and composition of the migmatitic granite host rock; the fault rocks exhibit mylonitization and cataclastic breccia fabrics. Hydrothermal fluid alteration transformed the biotite and plagioclase into chlorite. In addition to the precipitation of carbon-rich fluids, which resulted in the formation of graphite, the weaknesses of these fault rocks were compounded by the presence of clay minerals and their obvious cataclastic structures. The comprehensive effect of the geological characteristics of fault rock, geological structure, ground stress, and TBM excavation unloading leads to collapse and large deformation of the weak rock in the fault zone as the main geological reason for the TBM jamming; the corresponding engineering treatment measures and recommendations are proposed. This case aims to provide reference and learning for avoiding the re-occurrence of similar jamming accidents.

Keywords Fault rock · Migmatitic granite · Clay minerals · Graphite · TBM jamming

✉ Zhenhao Xu
zhenhao_xu@sdu.edu.cn

Peng Lin
sddxytjp@sdu.edu.cn

Tengfei Yu
201820460@mail.sdu.cn

Ruiqi Shao
shaoruiqi@mail.sdu.edu.cn

Wenyang Wang
sduwwy@163.com

¹ Geotechnical and Structural Engineering Research Center, Shandong University, Jinan 250061, Shandong, China

² School of Civil Engineering, Shandong University, Jinan 250061, Shandong, China

³ Suzhou Research Institute, Shandong University, Suzhou 215123, Jiangsu, China

⁴ School of Qilu Transportation, Shandong University, Jinan 250061, Shandong, China

Introduction

In engineering geology, a fault is often classified as a kind of structural plane that develops in the surrounding host rock. The changes caused by a fault depend on the fault length, depth, mode, orientation, tectonic stresses, and the nature of the host rock. For example, deep, laterally extensive fault zones often constitute seismological faults, which control the distribution of the tectonic stress field and the stability of the block and rock mass. Small and medium faults that occur in the shallow subsurface can have a significant impact on the layout and design of large engineering projects and the local stability of the engineering rock masses (Peng et al. 2004). Due to internal and external forces, the rock mass in the fault zone is loose and broken, with well-developed cracks and poor stability. Therefore, in tunnels and other underground engineering projects, the presence of faults can cause major construction setbacks such as water and mud inrush, collapse, and large-scale convergence deformation (Lin et al.

2017; Li et al. 2018; Xu et al. 2020a; Chen et al. 2020; Xue et al. 2020, b).

Determining the physical and mechanical properties of fault rocks requires analysis of the geochemical, mineralogical, petrological, and structural features of these fault rocks (Numelin et al. 2007; Bradbury et al. 2015). For example, the strength of the fault rock is inversely proportional to the clay content; furthermore, the distribution of the clay minerals within the fault will affect the degree of fault weakening (Chester et al. 1993; Moore et al. 2008; Holdsworth et al. 2011). As an important factor affecting the engineering geological characteristics of faults, the study of the physical and mechanical properties of these fault rocks provides valuable insights into the formation mechanism of the varying geological disasters caused by the existence of or motion along faults (Scholz 1987; Zhang et al. 2018, 2019).

Current research on the geological characteristics of fault rocks mainly focuses on cores collected during scientific drillings of seismic faults such as the Japan Nojima Fault Scientific Research Project in the Pacific Rim Seismic Belt (Matsuda et al. 2001, 2004; Tanaka et al. 2001), the Taiwan Chelungpu Fault Drilling Project (Lin et al. 2005; Isaacs et al. 2007; Hirono et al. 2008; Kuo et al. 2009), the San Andreas Fault Deep Observation Drilling Project (Schleicher et al. 2009; Holdsworth et al. 2011; Janssen et al. 2012, 2014), the New Zealand Deep Fault Drilling Plan (Schleicher et al. 2015; Warr and Cox 2001; Williams et al. 2017), and the Wenchuan Earthquake Fault Zone Scientific Drilling Plan (Chen et al. 2013; Li et al. 2013; Duan et al. 2016). These projects ultimately hope to quantify the effects of internal and external forces on the evolution of the fault zone by analyzing the geochemical compositions, mineral characteristics, and microstructural changes in the host and fault rocks. Once these features have been measured, the authors can then frame their conceptual model of the fault zone evolution and explore the fault zone deformation behavior and fracture mechanisms within that framework. However, very few of these projects use their analyses of the fault rock geological characteristics to ascertain the potential for geological disasters during engineering and construction processes.

When TBMs excavate tunnels in fault zones, the collapse of the tunnel face and roof often leads to TBM jamming (Xu et al. 2020a). Farrokh and Rostami (2009) concluded from the field and geotechnical investigations that weak rock masses, extensive foliated structures, and faults are the main causes of multiple TBM jamming accidents in the Ghomroud Tunnel, Iran. Bilgin (2016) analyzed engineering cases such as Kargi tunnel, Gereede tunnel, Dogancay energy tunnel, and Nurdagi Rail tunnel in Turkey and considered that the tremendous engineering geological problems such as TBM jamming and tunnel face collapse in the above projects occurred mainly affected by the north and east Anatolian

faults and secondary minor faults. The Zagros water transfer tunnel in Iran was excavated with a double-shield TBM in a fault zone where the unpredictable collapse occurred, which caused jamming of the cutter head and shield; Bayati and Hamidi (2017) proposed a detailed ground improvement and grouting technique for releasing the TBM. In addition, the weak rock mass in the fault zone or interlayer shear zone can also be subject to large deformation under high ground stress, which can lead to TBM jamming (Shang et al. 2004; Xu et al. 2020a). Zhang and Zhou (2017) established an advanced physical and mechanical model to characterize the interaction between the single-shield TBM and the surrounding rock, such as contact, squeeze, and friction, and reveal the time-dependent jamming mechanism. Bejari and Hamidi (2018) used semi-empirical methods and numerical models to evaluate the possibility of squeezing deformation of the stratum and combined with the constrained convergence method to determine the critical section where TBM jamming may occur. Aydan and Hasanpour (2019) proposed a displacement function related to facing distance, shield type, and rigidity to estimate the contact ground pressure and thus determine the likely location of the jamming. Liu et al. (2019) proposed a numerical simulation method based on modified Newton iteration for the inverse analysis of surrounding rock loads, which can effectively identify the distribution and magnitude of surrounding rock loads and take timely measures to avoid shield jamming based on the identified loads. Hasanpour et al. (2020) used Bayesian and artificial neural networks to assess shield TBM jamming risk in squeezing grounds.

The above researches focused on the theoretical analysis and numerical simulation methods to analyze the squeezing effect of the surrounding rock on the TBM from both mechanical and geometric perspectives and then determine the trigger conditions for the occurrence of the jamming accidents. Meanwhile, in the engineering geological analysis of specific jamming cases, there is still a lack of understanding of how the geological characteristics of fault rocks impact TBM jamming. In this study, we use optical thin sections, X-ray fluorescence spectroscopy, X-ray diffraction spectroscopy, and infrared carbon and sulfur analyses to determine the geological characteristics of the fault and host rocks in a tunnel of the central Yellow River Diversion in Shanxi. Our research results provide a basis for determining the geochemical changes and mineralogical transformations caused by faulting. By integrating the geochemical, mineralogical, and microstructural characteristics of the host and fault rocks, we obtained evidence for the weakening of the mechanical characteristics of the fault rock. Based on the analysis of geological structure, ground stress, and rock mechanics parameters, the engineering geological reasons for the occurrence of the TBM jamming are derived, and corresponding engineering treatment measures and

recommendations are proposed. The analysis of this case helps to raise awareness of the adaptability of double-shield TBM encountering reverse faults when excavating in granite and aims to provide reference and learning for avoiding the re-occurrence of similar jamming accidents.

TBM jamming hazards at mileage 106 + 402.8

The TBM2 bid section of the central Yellow River Diversion Project is located in Linxian County in Lvliang City in Shanxi Province (Fig. 1a). A double-shield TBM excavates the tunnel, and the entrance of the branch hole is located in Yangjiaya Village in Muguaping Township. With a total length of 20.326 km, the starting and ending mileage of the tunnel is from 118 + 395.8 to 98 + 070.2, respectively. The axial direction of the tunnel section from mileage 118 + 395.8 to 102 + 370.9 is N7.6°E, and the axial direction of the tunnel section from mileage 102 + 370.9 to 98 + 070.2 is N23.2°E (Fig. 1b). The ground elevation of this deeply buried, extra-long tunnel ranges from 1247 to 1580 m, and the buried depth of the bottom of the tunnel ranges from 255 to 589 m.

The TBM excavation step length is 1.4 m. The diameter of the tunnel is 5.06 m, and the construction section is circular. The tunnel lining adopts a segmental structure, which is made of precast C₄₅ concrete (uniaxial compressive strength larger than or equal to 45 Mpa and less than 50 MPa), with an outer diameter of 4.8 m, an inner diameter of 4.3 m, and a thickness of 25 cm. Four concrete segments form a ring, with a hexagonal honeycomb structure. An annular space exists between the excavated rock surface and the concrete ring, which is first filled with pea gravel and then backfilled with grout through the grouting port, and in the double-shield excavation mode, segment installation is completed during excavation.

On October 26, 2017, when the TBM excavated the tunnel to mileage 106 + 402.8, the cataclastic breccia on the upper left side of the cave wall collapsed and lead to the front shield jamming. After manually excavating the tunnel to mileage 106 + 391.8, the collapsed rock mass led to the cutter head jamming again. After performing chemical consolidation grouting on the front upper part of the cutter head and emptying the gravel on the right half of the cutter head, continued excavation was stalled when excessive torque caused the safety pin of the main motor to cut off multiple times. When the scalable shield was opened, granitic mylonite and cataclastic breccia burst into the shield (Fig. 2a), and the left front and rear shields were locked by debris from a nearby collapse (Fig. 2b). The groundwater in the cave section from mileage 106 + 410 to mileage 106 + 391 is metamorphic rock fissure water and

Cambrian–Ordovician carbonate rock fissure karst water, with only a small amount of groundwater actively seeping out of the host rock.

Engineering geological conditions

Regional geology

Figure 3 shows the simplified regional geological structure map of our study area. The tunnel site is located in the first-level structural unit of the eastern margin of the Ordos Basin; this unit is a flexural fold belt located west of Shanxi. As the Yanshan Movement uplifted and pushed the Lvliang Mountain to the west, a flexural fold belt in Shanxi formed along a basement fault. This fold belt is characterized by a near N-S trend and numerous short-axis folds. The east side of this fold belt is adjacent to the Shanxi fault uplift and is bounded by the Lishi fault, which is a crustal-scale boundary fault. The whole fault is located on the west side of the Lvliang Mountains and extends from Jiaolou Shen township in Xing County in the north, passing through the Heicha Mountain in the south, extending from the east of Hango Mountain in Lin County to the west of Yukou township in Fangshan County, and then from Matou Mountain in the south through Zhongyang County to Jiaokou County, and finally extending in the direction of Linfen, stretching a total of 270 km from north to south (Liao et al. 2007). The TBM 2 section is located on the west side of the Lishi fault.

Engineering geology characteristics

Figure 4 shows the engineering geological cross-section of the TBM 2 bid section. The ground surface of the tunnel is largely covered by loose Quaternary deposits, and the bedrock is only exposed at the bottom or the sides of the gully. The tunnel crosscuts the Archean Jiehekou Group Aojiawan Formation (Ar_{2a}), the Lower Proterozoic Heichashan Group (Pth), and the Paleozoic Cambrian (C), and Ordovician (O); these strata consist of biotite plagioclase gneiss, granitic gneiss, granitic pegmatite, quartzite, dolostone, and limestone. The geological structure of the tunnel site area is complex, and instances of migmatization are prominent. Along the tunnel route, there are three anticlines, three synclines, and nine large-scale faults (Fig. 4). Before the TBM tunnel was excavated to mileage 106 + 410, the exposed stratum was dolomitic limestone from the Middle Cambrian Zhangxia Formation with the occurrence N21°E/NW18–21°. When the excavation reached mileage 106 + 410, the amount of migmatite and cataclastic breccia on the left side of the tunnel increased markedly. In addition to the exposure of fault FT₂, graphitized cataclastic breccia and chloritized migmatitic granite began to appear on the

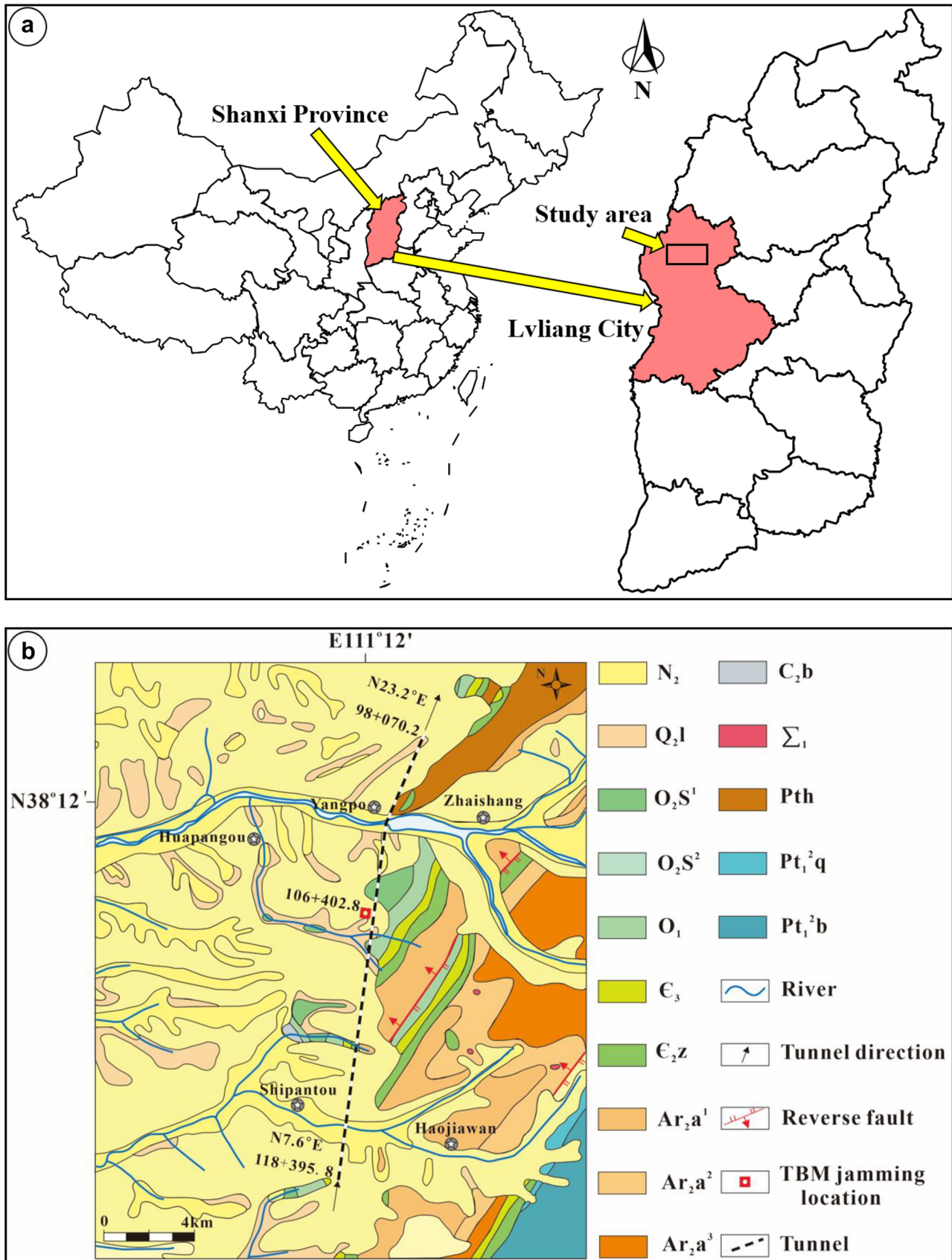
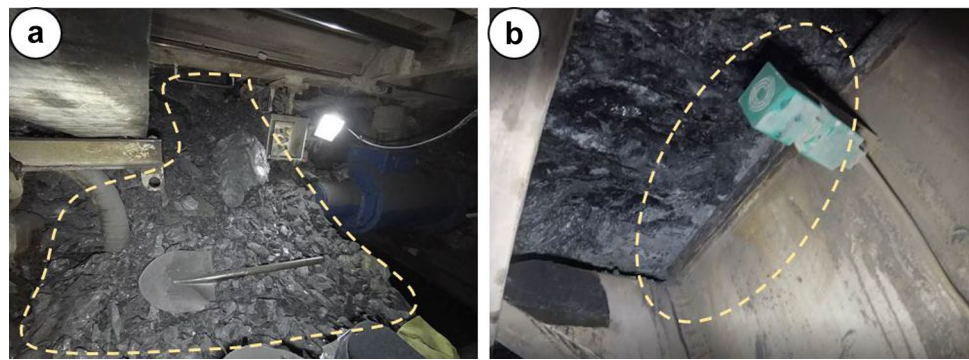


Fig. 1 Geographical location and simplified geological map of the study area. a Geographical location map. b Simplified geological map

Fig. 2 Photographs of TBM jamming. **a** Fractured fault rock. **b** TBM jamming caused by the collapse of the fault rock



left side of the tunnel face once the tunnel was excavated to mileage 106 + 405. The geological cross-section of the FT₂ fault zone is shown in Fig. 5.

With a strike of N20-30°E and a dip of NW75°, FT₂ is a thrust fault that exhibits extrusion and torsion. The Archean Aojiawan Formation stratum on the hanging wall has been thrust upwards to an elevation above the tunnel line, and the strata in the footwall are comprised of Cambrian sandstone and dolomitic limestone from the Cambrian Zhangxia Formation. The Cambrian sandstone overlaps and was deposited on the underlying Archean Aojiawan Formation, creating an angular unconformity contact. The FT₂ fault is confined

to the ancient, weathered crust that underlies this contact zone. Due to fault extrusion, the fault rock exhibits lenticular fragmentation, and its surface is characterized by graphitization and mylonitization. Graphitization causes the host rock surface to be covered in flaky layers. The greasy and smooth surfaces of the rock are silver-gray-black and are covered with long linear scratches; altogether, it is nearly impossible to observe the characteristics of the host rock (Fig. 6).

The main physical and mechanical parameters of the host rocks are shown in Table 1. The saturated uniaxial compressive strength of the dolomitic limestone of the Middle Ordovician Zhangxia Formation (E_{2z}) on the footwall is

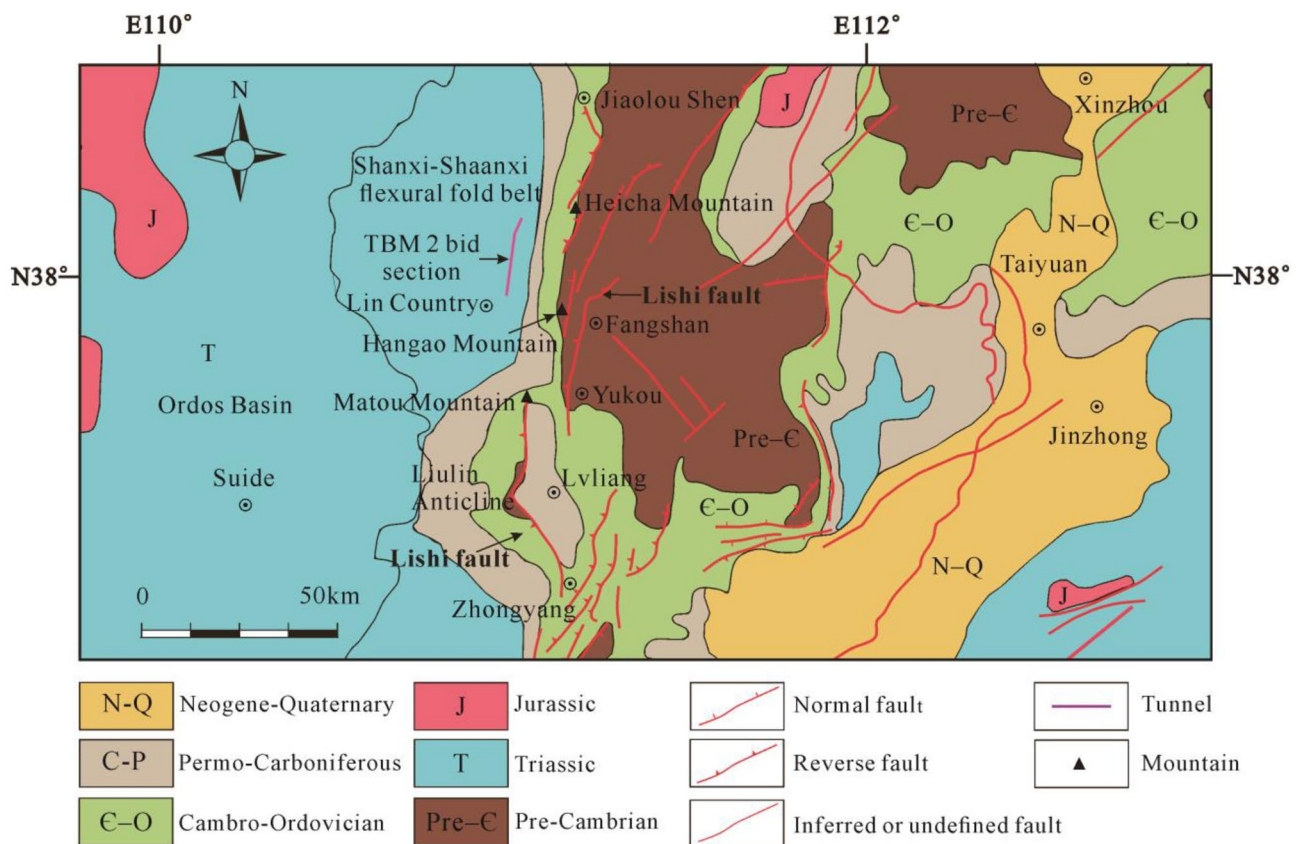


Fig. 3 Simplified regional geological structure map (modified after Liao et al. 2007). The TBM 2 bid section is denoted by the purple line

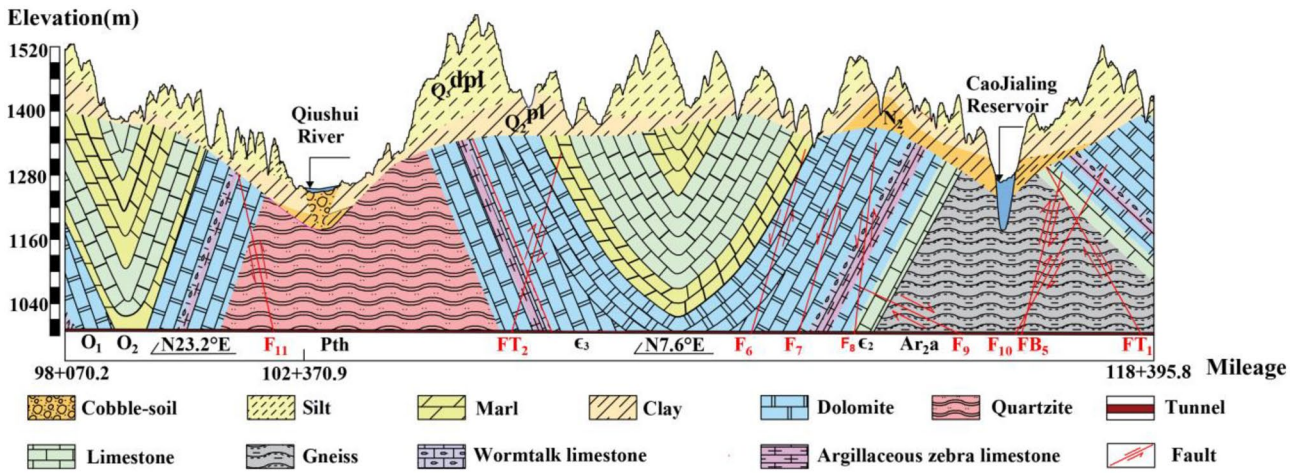


Fig. 4 Engineering geological cross-section of TBM 2 bid section

39.7–62.4 MPa, the deformation modulus is 30.9–49.6GPa, and the average value of RQD is 52. The saturated uniaxial compressive strength of the granite of the Aojiawan Formation (Ar₂a) on the hanging wall is 30.3–37.6 MPa, the deformation modulus is 31.1–49.0 GPa, and the average value of RQD is 47. Considering the effects of groundwater and discontinuity face, the RMR scores of the dolomitic limestone and granite are 49–52 and 44, respectively, and both are classified as grade III rock mass (corresponding to the RMR89 rock mass rating score of 41–60).

Figure 7 shows rose diagrams of the rock joints, four groups of joints are mainly developed in the stratum along the tunnel and are mostly filled with calcite. The

strikes of joints are set in N20°–50°W/NE∠75°–85°, N5°–35°W/SW∠60°–85°, N70°–83°W/SW∠75°–85°, and N65°–85°E/NW∠70°–85°, respectively (Fig. 7). The spacing of joints ranges from 0.5 to 3 m, and the width of joints ranges from 0.5 to 5 mm. Figure 8 shows the variation curves of different ground stress components with depth measured by hydro-fracturing in the borehole ZK12ZT-8 at mileage 92 + 810.64. The maximum horizontal principal stress value is 17.6–20.19 MPa with the azimuth N82°–86°E, the minimum horizontal principal stress value is 10.58–12.95 MPa, and the vertical principal stress value is 14.42–19.11 MPa. Each principal stress component increases with depth, and the vertical principal

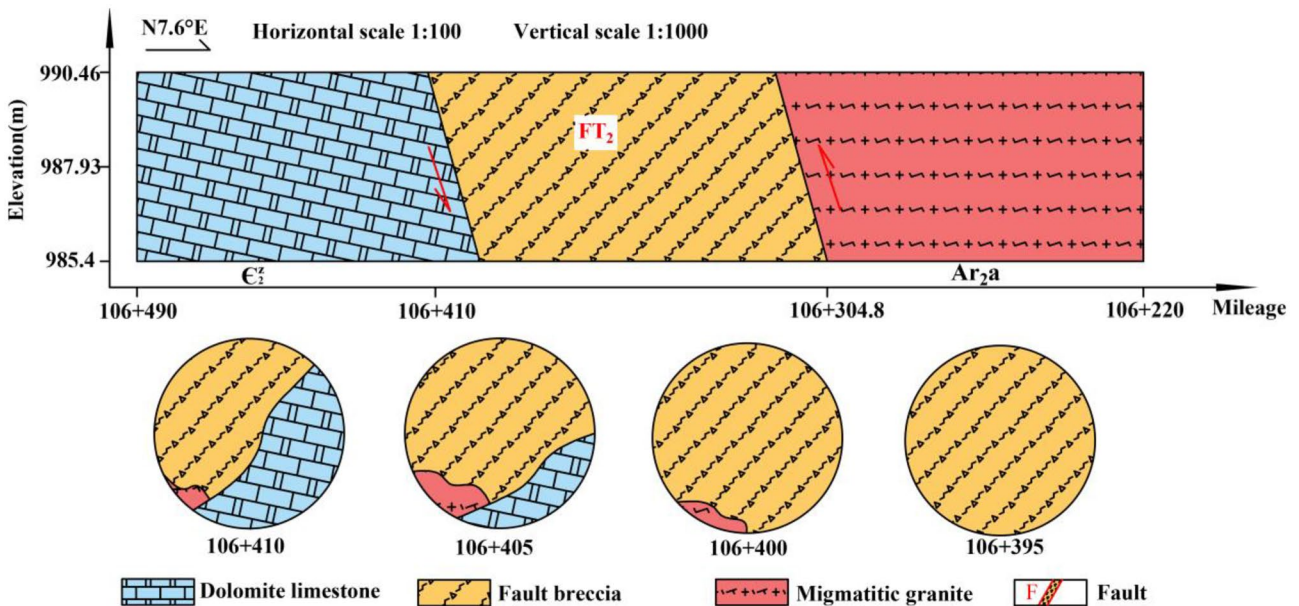
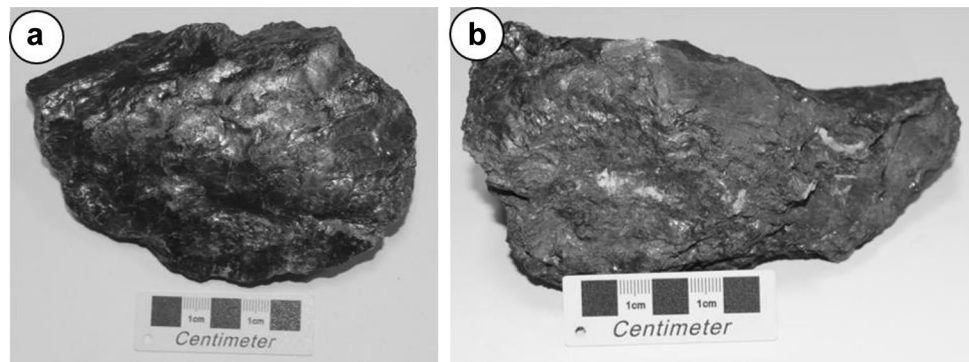


Fig. 5 Geological cross-section of the FT₂ fault zone

Fig. 6 Samples of **a** mylonite and **b** cataclastic breccia taken from the FT₂ fault



stress in the test depth is the intermediate principal stress, that is, $S_H > S_v > S_h$. The burial depth of the tunnel in the section of TBM jamming is about 465 m. It can be seen from Fig. 8 that the maximum horizontal principal stress, vertical principal stress, and minimum horizontal principal stress values in this section are 19.75 MPa, 17.94 MPa, and 12.81 MPa, respectively.

Microstructural, geochemical, and mineralogical characteristics of the fault and host rocks

The microstructural characteristics, component changes, material migration, and transformation processes of a given rock can be determined by observing its microstructures under a microscope (Xu et al. 2021a, b). The lithology of and analytical methods applied to the fault and host rocks at tunnel mileage 106 + 402.8 are shown in Table 2.

Microstructural characteristics of the fault and host rocks

Cataclastic granite in the hanging wall

Due to fault compression, intragranular, intergranular, and transgranular microfractures formed in the granite host rock. These transgranular microfractures are gradually filled with carbonate minerals that form normal and reticular veins.

There appears to be no displacement between the larger granite fragments and the granite breccias; overall, the rock has a cataclastic fabric (Fig. 9a). The main minerals in this rock are quartz, plagioclase, microcline, mica, and calcite. These round to granular quartz grains, which exhibit strong undulatory extinction, are irregularly distributed in the interstices of the feldspar grains, with grain sizes ranging from 2 to 6 mm. Cracks in these quartz grains are filled with calcite. Plagioclase grains with a hypidiomorphic tabular texture have lengths of 3–6 mm and occasionally exhibit polysynthetic twinning. Most plagioclase crystals have been sericitized. Cracks in some plagioclase grains are filled with calcite micro-veins. Pyrite grains, which have mostly been crushed by tectonic stresses, are irregularly distributed in the fractured cracks of the host rock and have grain sizes of 0.02–0.5 mm (Fig. 9b).

Graphitized granitic mylonite

The main mineral components of the graphitized granitic mylonite are feldspar and quartz; due to fracturing, fault slip, and fault shear, these rock and mineral components are characterized by plastic deformation and directional distribution (Fig. 9c). In these rocks, graphite exists either within veins or as distinct flaky deposits (diameter of 0.05 mm to 1.5 mm) that have a straw yellow reflection color and exhibit obvious double reflection and strong heterogeneity under a microscope (Fig. 9d). Pyrite is irregularly granular, occurs in sparse disseminated and intermittent veins, and has grain

Table 1 Physical and mechanical parameters of the host rocks

Rock		Density/g·cm ⁻³		Uniaxial compressive strength/MPa	Deformation modulus/GPa	Poisson's ratios	Softening coefficient	RQD/%	RMR scores
		Nature	Saturation						
Dolomitic limestone	Variation range	2.77–2.80	2.79–2.81	39.7–62.4	30.9–49.6	0.18–0.24	0.90–0.92	6–91	49–52
	Average	2.79	2.8	51.1	40.3	0.21	0.91	52	
Granite	Variation range	2.55–2.63	2.56–2.66	30.3–37.6	31.1–49.0	0.12–0.23	0.58–0.87	9–93	44
	Average	2.59	2.61	34	40.1	0.18	0.73	47	

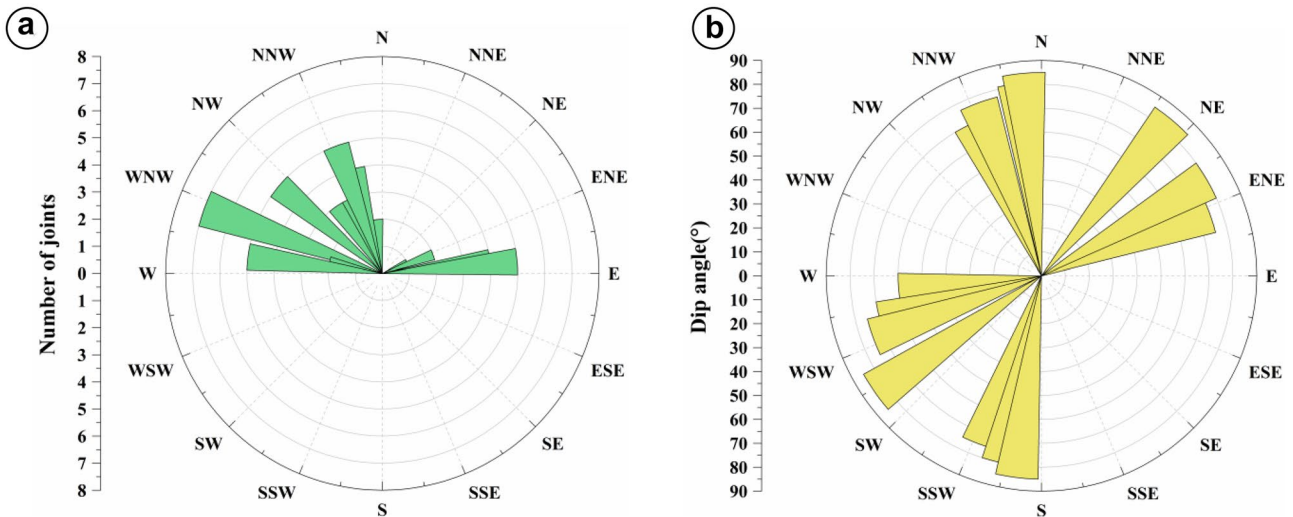


Fig. 7 Rose diagrams of joint. **a** Rose diagram of joint direction. **b** Rose diagram of joint inclination and dip angle

diameters between 0.03 and 0.6 mm. The highly sericitized plagioclase grains are elliptical in shape and have grain diameters between 0.2 and 0.6 mm (Fig. 9e). The quartz grains have irregular shapes and grain sizes ranging from 0.03 to 0.5 mm. Some recrystallized podiform and banded quartz grains are directionally distributed throughout the rocks. Interstitial flaky mica grains have diameters of 0.1 to 0.4 mm; some of these grains have been altered into chlorite (Fig. 9f).

Pyritized granitic cataclastic breccia

The main mineral composition of the granitic cataclastic breccia is feldspar and quartz. Due to multiple stages of tectonic activity, the earlier consolidated rocks were crushed and cut by later tectonic events to form tectonic breccias and porphyroclasts. The tectonic breccia and porphyroclasts are composed of highly fragmented feldspar and quartz (55–60%) (Fig. 9g). The breccia fragments have diameters

Fig. 8 Measured ground stress components at different depths of the ZK12ZT-8 borehole. S_H , maximum horizontal principal stress; S_h , minimum horizontal principal stress; S_v , vertical principal stress

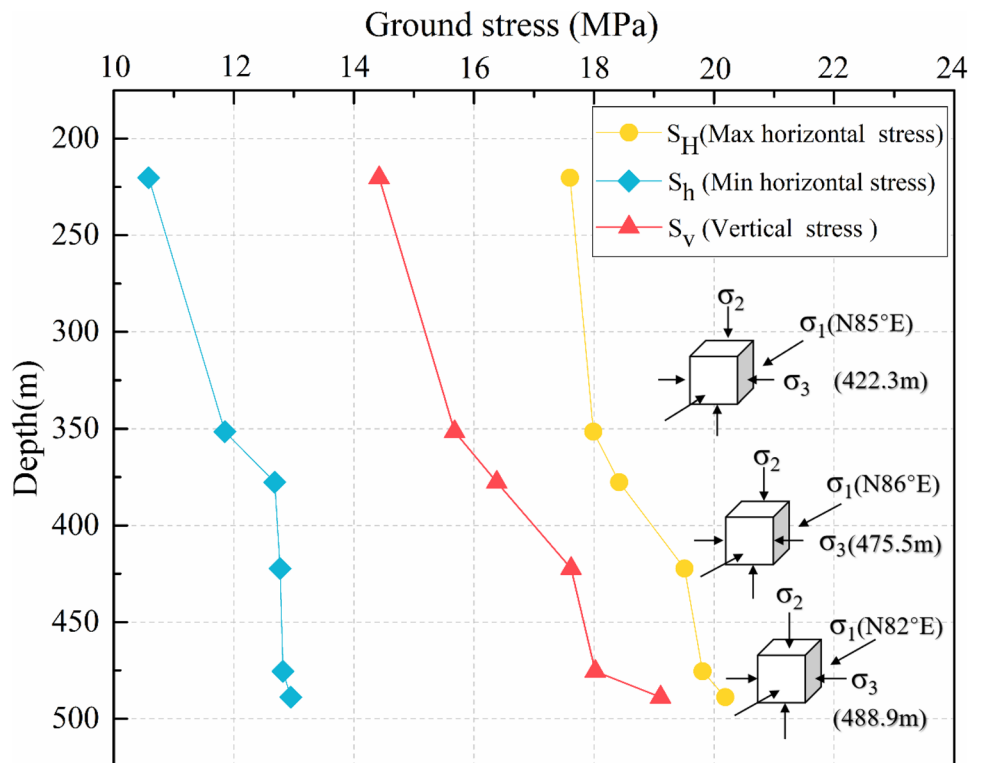


Table 2 Lithology and locations for samples taken from tunnel mileage 106 + 402.8

Sample name	Location collected	Lithology	Analysis in this study
S-01	The footwall of the FT ₂ fault	Migmatitic granite	Thin section, XRF, XRD
S-02	Within the FT ₂ fault zone	Graphitized granitic mylonite	Thin section, XRF, XRD, ICSA
S-03	Within the FT ₂ fault zone	Pyritized granitic cataclastic breccia	Thin section, XRF, XRD, ICSA

ICSA: (Infrared carbon and sulfur analysis)

of 2–5 mm, and the porphyroclastic fragments have diameters of 0.5–2 mm. The veins in the breccia and porphyroclast fragments are filled with calcite and chlorite. The matrix largely consists of powder and debris (36–42%) with a particle size of 0.01–0.5 mm. The secondary matrix component is gray-black powdery carbon-bearing material that is distributed throughout (and acts as cement between) the interstices of the tectonic breccia and porphyroclast fragments. While most of the pyrite occurs in crushed irregular grains, it sometimes occurs as cubic crystals with a grain size of 0.01–0.5 mm. These pyrite grains are largely located in cracks and pores in the form of sparse disseminated and intermittent veins (Fig. 9h).

Element losses and gains in fault rock

After the rock samples were crushed and ground to a particle size of less than 200 mesh, we measured the main and secondary oxide contents (including Na₂O, MgO, Al₂O₃, SiO₂, P₂O₅, K₂O, CaO, TiO₂, MnO, and Fe₂O₃* [total Fe₂O₃]) of the fault rock using a ZSXPrimusIV X-ray fluorescence spectrometer. The volatile component (LOI) was measured via the thermo-gravimetric analysis method (Tanaka et al. 2001). The element behavioral changes observed in the fault zone can be divided into three categories: the aggregate component series, the discrete component series, and the mean component series (Xu et al. 2021c). The aggregate component series is more enriched than the host rock, the discrete component series is more depleted than the host rock, and the mean component series is very similar to the host rock (Tanaka et al. 2001; Sun et al. 1998; Duan et al. 2016). The element content values for our rock samples are shown in Fig. 10.

While the Na₂O, CaO, and SiO₂ contents of the FT₂ fault rocks are relatively depleted compared to that of the host migmatitic granite (Fig. 10), the LOI is higher in the fault zone than it is in the host rock. The LOI enrichment in the fault zone reflects the existence of interlaminar bound water in certain phyllosilicate minerals (Isaacs et al. 2007; Duan et al. 2016; Niwa et al. 2019). The migration and change law of these oxides and volatiles across the fault zone are restricted by tectonic geochemistry-dynamic differentiation. With large ionic radii and small specific gravities, Na and Ca are more likely to be lost during tectonic compressional stress (Sun et al. 1998). Both the higher MgO, Fe₂O₃*

and Al₂O₃ content and the enrichment of chlorite in the graphitized granitic mylonite are related to the inclusion of magnesium-rich and iron-rich fluids in the plagioclase alteration process "Enrichment characteristics and sources of clay minerals in fault rocks".

In the pyritized granitic cataclastic breccia, we found that MgO is relatively enriched, Al₂O₃ is relatively depleted, and there is a slight loss of CaO (Fig. 10). These observations may be caused by the presence of veins filled with reticulated carbonate minerals in the breccia and porphyroclastic fragments "Pyritized granitic cataclastic breccia". The P₂O₅ in the fault rock can be categorized as the mean component series. The geochemical changes in the FT₂ fault zone rocks indicate that fluid–rock interactions and hydrothermal alteration have played a significant role in the alteration of these rocks (Matsuda et al. 2004; Isaacs et al. 2007; Niwa et al. 2019).

Enrichment characteristics and sources of clay minerals in fault rocks

The FT₂ fault rocks are rich in graphite and clay minerals. The presence of these minerals significantly reduces the rock strength and, therefore, the stability of the tunnel. Because the formation of the aforementioned minerals is usually related to the fluid–rock interaction, it is useful to explain how the geochemical and microstructural characteristics of the fault rocks inform the rock formation and transformation processes that ultimately result in TBM jamming. We performed mineral analyses on our samples using a Rigaku Dmax-RB type rotary anode X-ray diffractometer with a graphite monochromator, CuK α radiation, an X-ray tube voltage of 40 kV, a scanning step length of 0.02°, and a scanning range of 3°–70°. Our XRD whole-rock mineral analyses are shown in Figs. 11 and 12.

The cataclastic granite on the fault hanging wall is composed of chlorite, mica, quartz, plagioclase, and microcline, with lesser amounts of calcite and pyrite. These observations are consistent with the results discussed in the "Microstructural characteristics of the fault and host rocks". The graphitized granitic mylonite in the fault is rich in chlorite and pyrite, and the pyritized granitic cataclastic breccia is rich in calcite, pyrite, and gypsum. The presence of pyrite, gypsum, calcite veins, and chlorite minerals indicates that

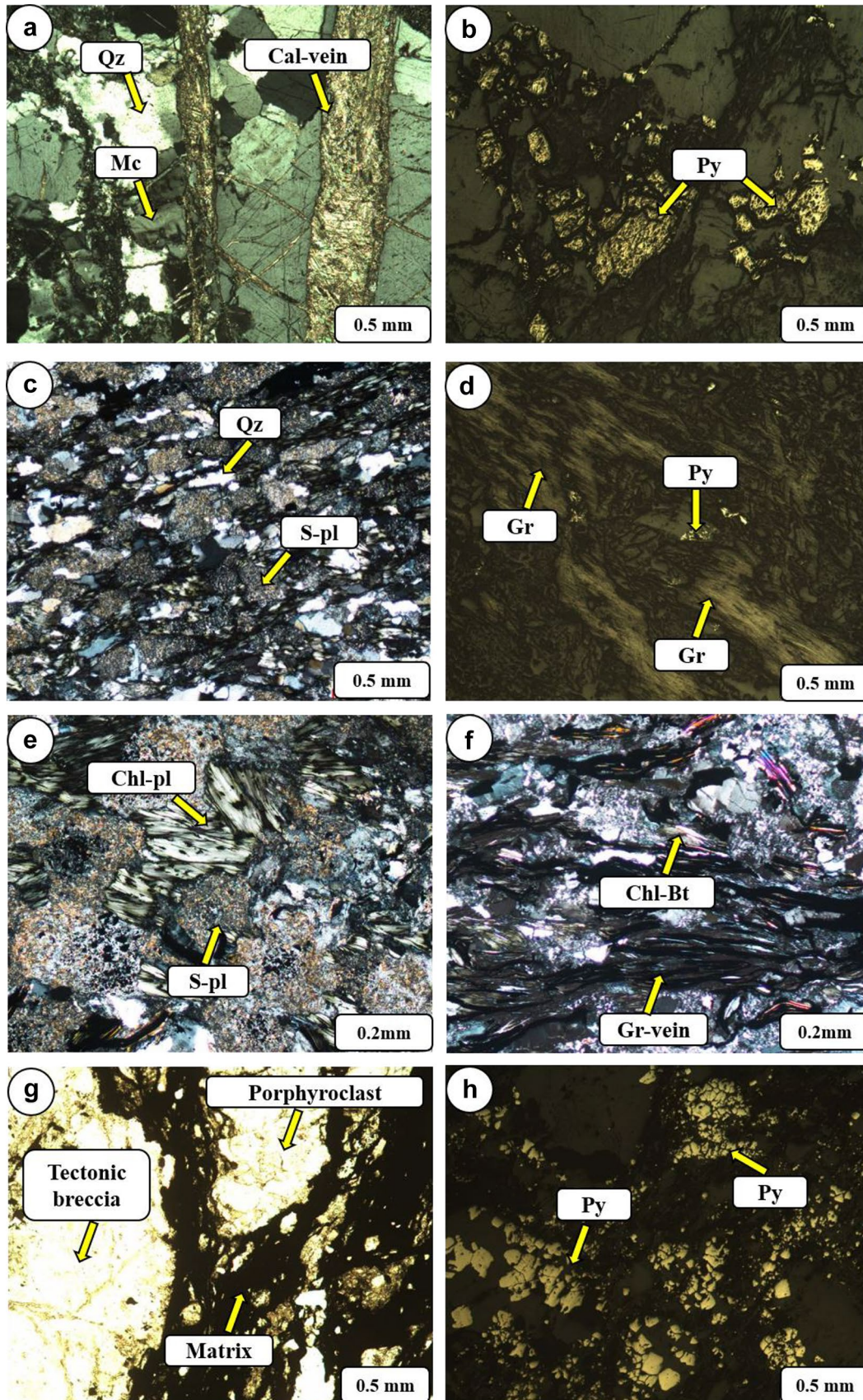
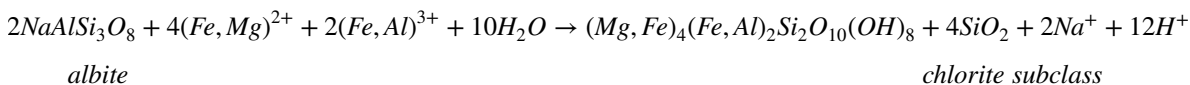
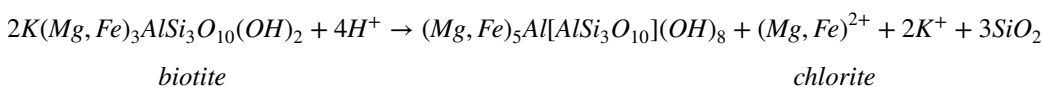


Fig. 9 Microstructures in the host and fault rocks collected from the FT₂ fault. **a** Cataclastic granite (cross-polarized light). **b** Granular pyrite in cataclastic granite (reflected light). **c** Graphitized granitic mylonite (cross-polarized light). **d** Flaky graphite in mylonite (reflected light). **e** Alteration of plagioclase in mylonite (cross-polarized light). **f** Vein-shaped graphite and altered biotite in mylonite (cross-polarized light). **g** Pyritized granitic cataclastic breccia (plane-polarized light). **h** Irregular granular pyrite in cataclastic breccia (reflected light). Cal-vein, calcite veins; S-Pl, sericitization of plagioclase; Chl-Pl, chloritization of plagioclase; Chl-Bt, chloritization of biotite; Gr-Vein, vein-shaped graphite

hydrothermal fluids have strongly influenced the evolution of the FT₂ fault zone (Duan et al. 2016). As shown in Fig. 12, the 002 and 004 diffraction peaks of chlorite in the fault zone sample are higher than the 001 and 003 diffraction peaks, indicating the presence of Fe-rich chlorite (Abd Elmola et al. 2017). Compared to amesite, the formation of daphnite requires lower oxygen fugacity conditions; the presence of daphnite indicates that the fluid–rock interaction occurred in a reducing environment (Trincal et al. 2014), as confirmed by the presence of pyrite. Furthermore, the presence of these hydrothermal minerals indicates that the fluid in the fault is rich in Fe, S, and Mg. Haines and van der Pluijm (2012) proposed that when host rocks are rich in magnesium, or when the hydrothermal fluids are rich in Fe and Mg, the new clay minerals in the fault zone should be chlorite or chlorite-rich. Based on our microscope observations "Microstructural characteristics of the fault and host rocks" and these XRD results, we infer that the chlorite in the FT₂ fault forms from the Fe and Mg components in the metasomatically altered plagioclase (Fig. 9e) or the alteration of biotite (Fig. 9f). Based on previous work (Duan et al. 2016), the chemical reactions related to the formation of chlorite are:



Enrichment characteristics and sources of graphite in the fault rocks

Many natural faults, such as the Spanish Central fault, the Japanese Atotsugawa fault, the Sichuan Longmenshan fault zone, the fault zones of the Hidaka metamorphic belt in Japan, and the Ailaoshan-Red River strike-slip fault zone in Southeast Asia contain graphite materials (Crespo et al. 2005; Oohashi et al. 2012; Kuo et al. 2014; Nakamura et al. 2015; Lyu et al. 2020). Studies have shown that graphite

materials usually exist in low- to high-grade metamorphic fault rocks as veins, lumps, flakes, and/or amorphous/microcrystals (Crespo et al. 2005; Oohashi et al. 2012; Nakamura et al. 2015; Cao and Neubauer 2019; Lyu et al. 2020). Different types of graphite materials can be found in brittle deformed cataclastic rock, fault gouge, and ductile deformed mylonite (Oohashi et al. 2012; Haertel et al. 2013).

Based on our microscope observations, we see that the cataclastic granite has no graphite material (Fig. 13a), the granitic mylonite in the FT₂ fault contains more vein and flaky graphite (Figs. 13b and 9d), and the granitic cataclastic breccia contains more interstitial carbon material (Fig. 13c). To determine the graphitic carbon content of the three rock samples, we used dilute hydrochloric acid to remove the inorganic carbon and filtered the remaining liquid to isolate the residue. Next, we washed and dried the residue with deionized water, followed by igniting the residue at 425 °C to remove any organic carbon. Using a LECO carbon–sulfur analyzer, we determined that the graphitic carbon content of the remaining residue for samples S-01, S-02, and S-03 was 0%, 3.97%, and 1.69%, respectively (Fig. 14).

There are two possible mechanisms for the enrichment of graphite materials in fault zones: (1) the precipitation of graphite materials from fluids rich in CO₂, CO, or CH₄ and/or mixed fluids containing carbon and water in the crust or (2) the creation of insoluble graphite material due to pressure dissolution or the general diffusive mass transfer that occurs when water-soluble minerals such as quartz and carbonate are dissolved and removed with water. The graphite formed by the second mechanism is usually related to the development of stylolite or pressure solution foliations (Oohashi et al. 2012; Lyu et al. 2020). However, because we do not observe graphitic carbon in the host

rocks or stylolite or pressure solution foliations in the fault rock, it is unlikely that the graphite material enrichment in the fault zone is caused by the pressure solution/diffusive mass transfer mechanism. The widely distributed veined graphite in the FT₂ fault is controlled by the rock structure, indicating that graphite originates from the isomorphic channel of the carbon-rich fluid passing through the fault zone (Oohashi et al. 2012; Craw and Upton 2014). Overall, we propose that the graphite in the FT₂ fault is related to the precipitation of carbon-rich fluids.

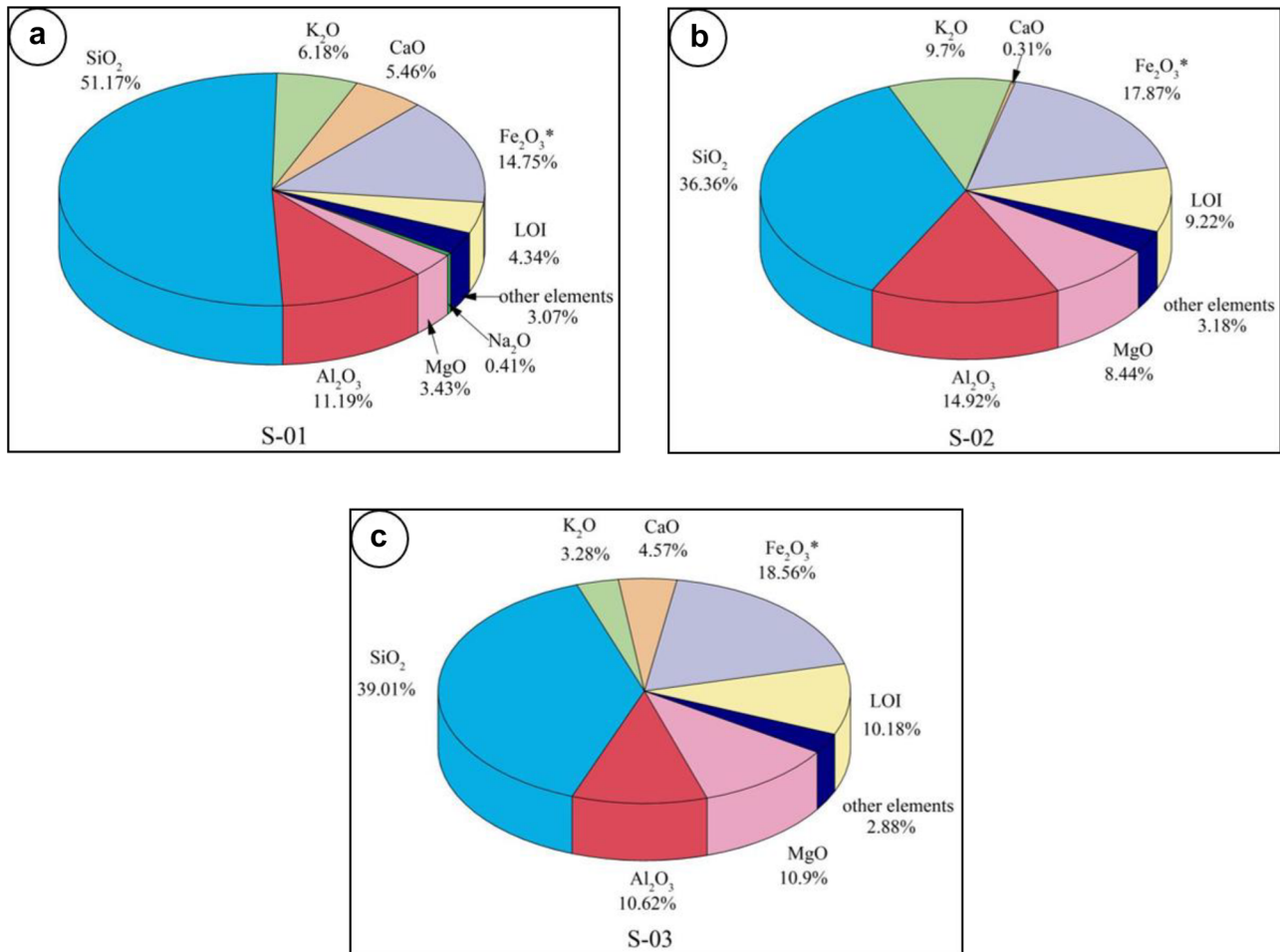


Fig. 10 The content of main migrating elements in rock samples. **a** S-01. **b** S-02. **c** S-03

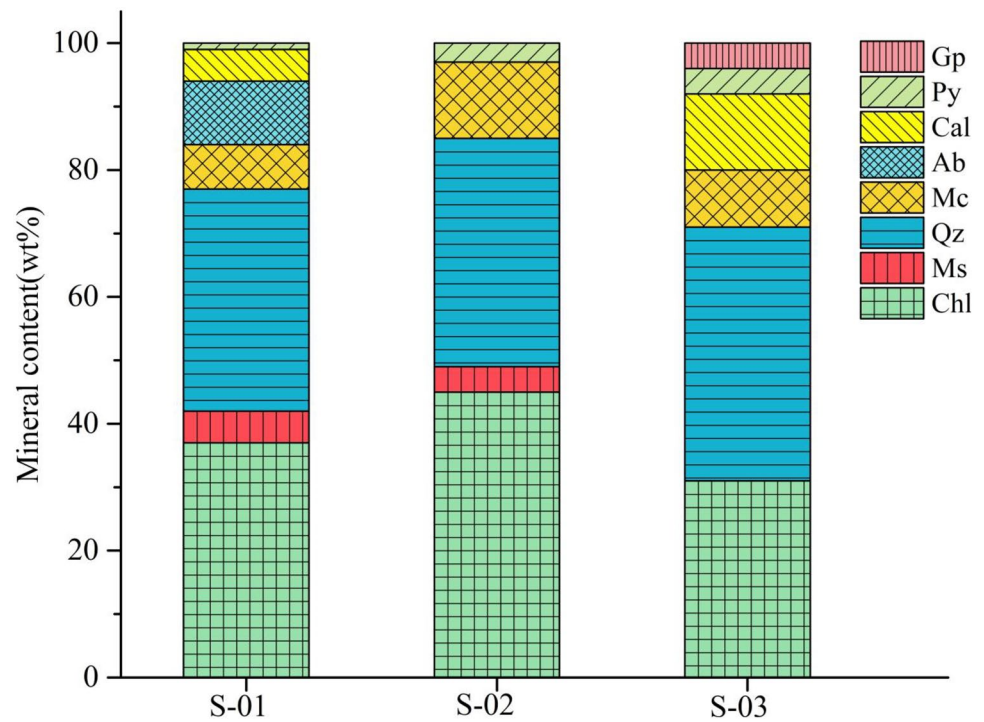
Fault rock characteristics

A comparative analysis of the microstructural, geochemical, and mineralogical characteristics of the host and fault rocks shows that long-term mechanical fracturing and geochemical effects have heavily altered the structure and composition of the migmatitic granite rock. The existence of both the ductilely deformed mylonite and the brittlely deformed cataclastic breccias in the FT₂ fault indicates that the fault zone has experienced one or more instances of structural deformation and superimposed reconstruction. The biotite and plagioclase in the fault were transformed into chlorite due to long-term hydrothermal alteration; the precipitation of carbon-rich fluids created veined and flaky graphite, which ultimately formed mylonite and cataclastic breccia during multiple tectonic events.

Combining the geochemical, mineralogical, and microstructural characteristics of host and fault rocks, the properties of fault rocks have been significantly weakened compared to granite after alteration, which is mainly

reflected in the following two aspects: (1) tectonic stress and long-term hydrothermal alteration lead to the development of rock fissures and pores and the disappearance of hard minerals such as albite. The residual quartz and microcline are loosely granular in the fault rocks, and the particle size is greatly decreased. The cementation between the mineral particles is weakened, and the integrity of the rock body is worsened in the macroscopical scale, showing a loose cataclastic texture (Fig. 9). (2) The biotite and plagioclase in the fault rock were altered to chlorite by hydrothermal alteration (Fig. 9), and chlorite, as a layered silicate, is easily softened and disintegrated when it was subjected to water. Carbon-rich fluids precipitate vein, flake, and dusty graphite, which as a solid lubricant slides as easily as other clay minerals in the (001) plane and can weaken the frictional strength of fault rocks (Oohashi et al. 2011; Nakamura et al. 2015; Cao and Neubauer 2019). The combination of chlorite and graphite can significantly reduce the stability of fault rocks than a single clay mineral.

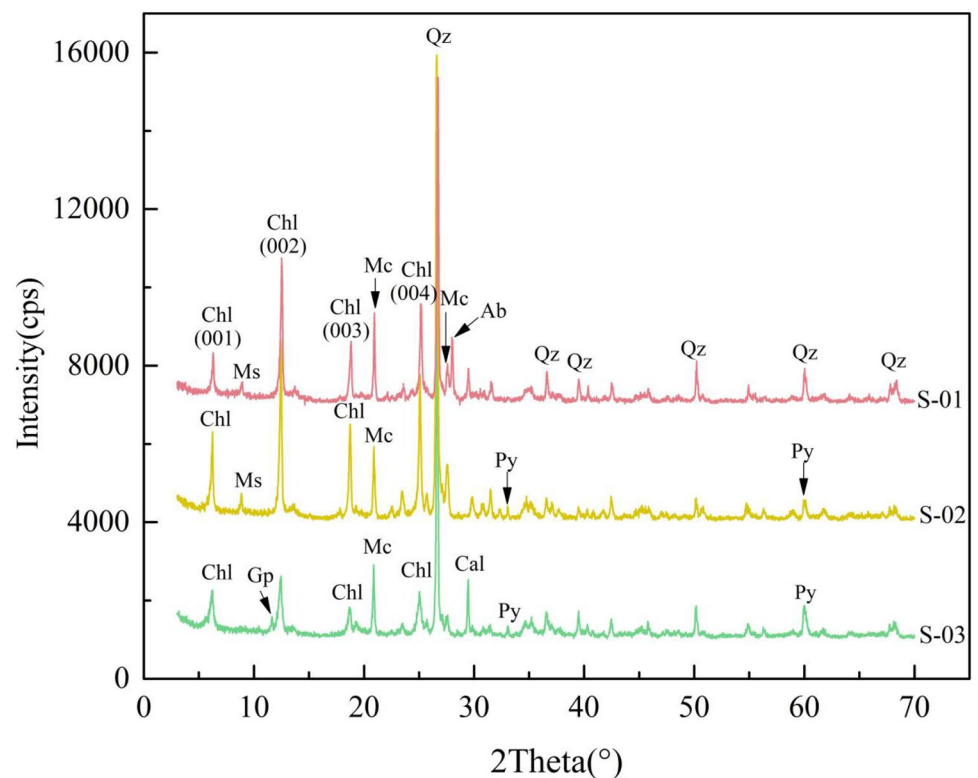
Fig. 11 Mineral content in the rock samples. Mineral content in the rock samples. GP, gypsum; Py, pyrite; Cal, calcite; Ab, albite; Mc, microcline; Qz, quartz; Ms, muscovite; Chl, chlorite



Noteworthy, the cataclastic breccia and mylonite in the fault core are formed by the granite on the hanging wall subjected to long-term tectonic stress and geochemical action. The uniaxial compressive strength of granite is 30.3–37.6 MPa, and the minimum uniaxial compressive strength of fault rocks will

be lower than 30 MPa or even lower because of the properties of fault rocks are weakened compared with the host rock, so fault rocks may be classified as soft rock. Therefore, at the local ground stress concentration of the inverse fault FT₂, the fault rock will likely be subjected to large deformation.

Fig. 12 XRD patterns of the rock samples. Qz, quartz; Chl, chlorite; Ms, muscovite; Ab, albite; Mc, microcline; Py, pyrite; GP, gypsum; Cal, calcite



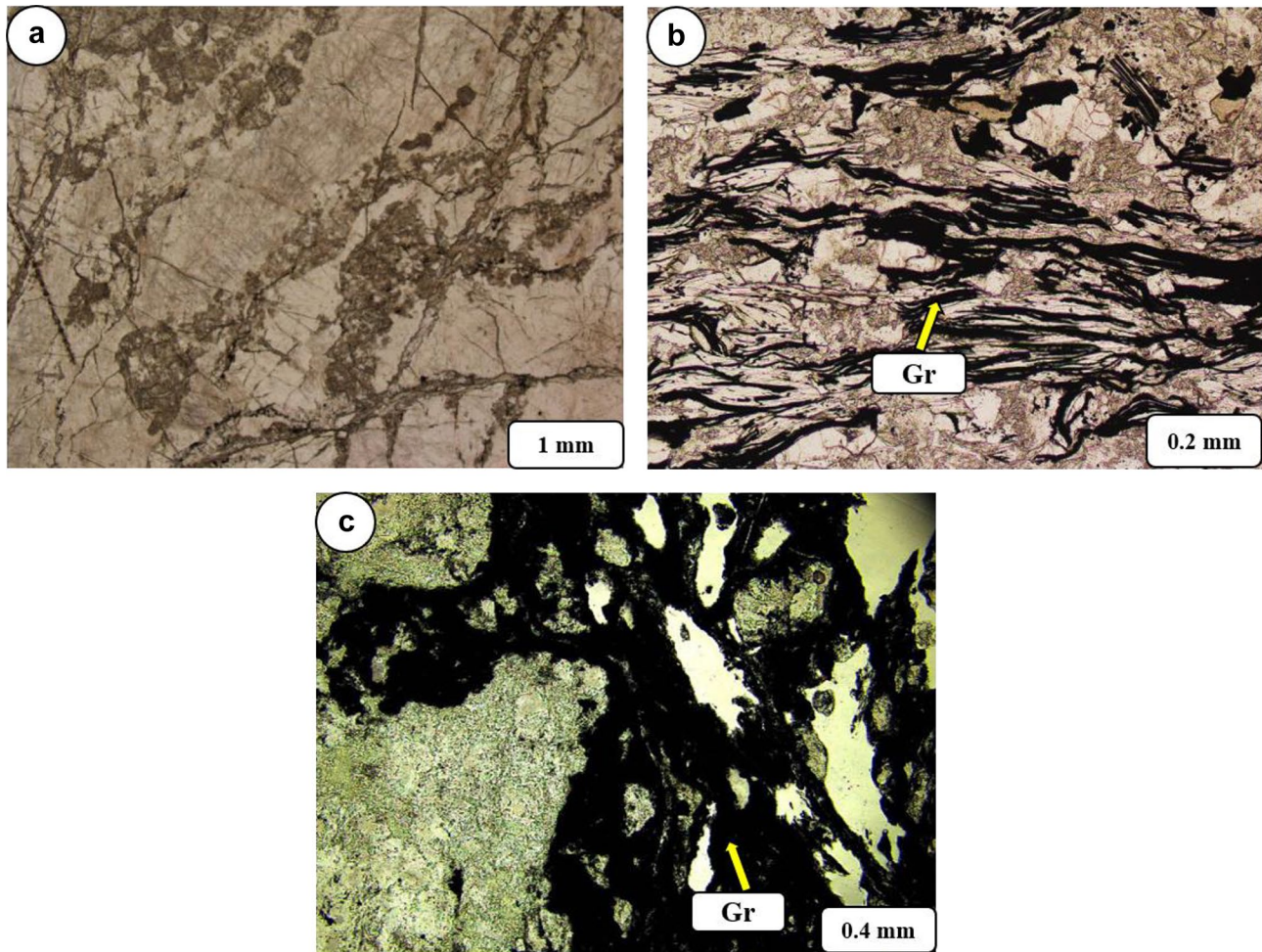


Fig. 13 The graphite carbon distribution characteristics found in our samples under plane-polarized light. **a** S-01. **b** S-02. **c** S-03

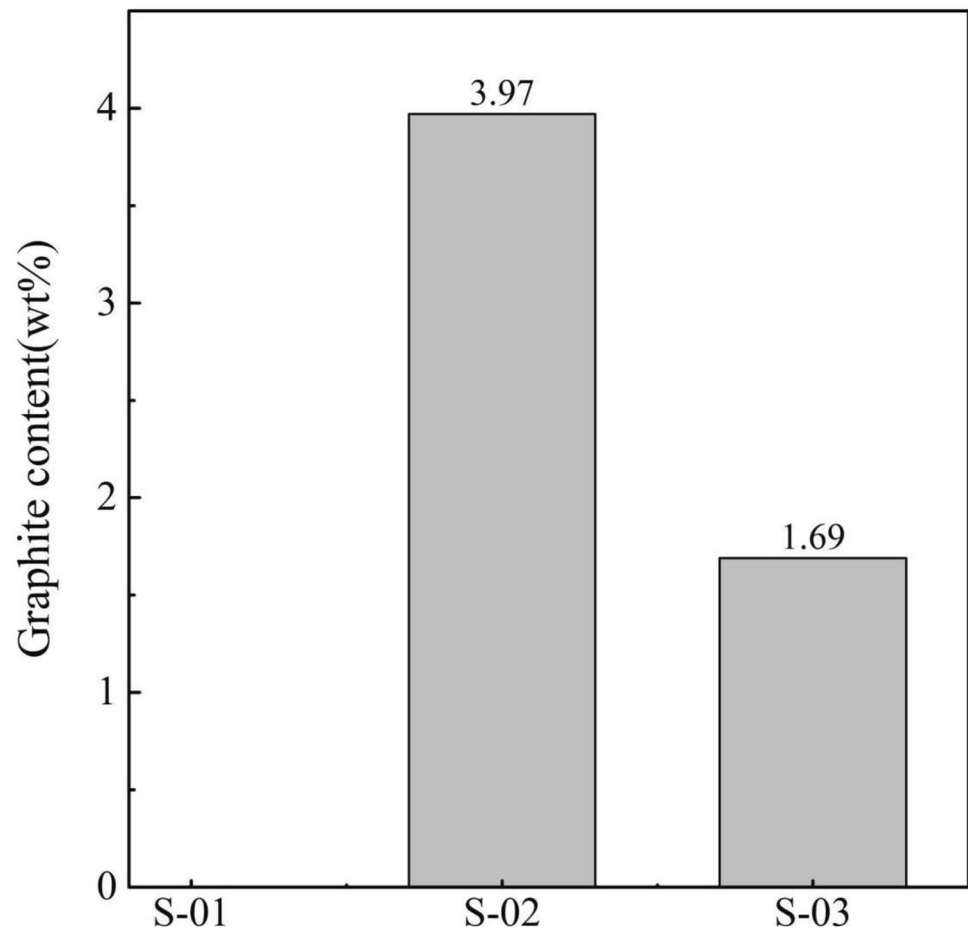
Engineering geological analysis, treatment measures, and recommendations for TBM jamming hazards

Engineering geological causes of the jamming accidents

For the integrated analysis of geological structures, ground stresses, host rock mechanical parameters, and geological characteristics of fault rocks, the main factors for the occurrence of TBM jamming are as follows:

- Characteristics of fault rocks: the fault rocks have typically cataclastic breccia and mylonite fabrics. Rich in clay minerals chlorite and “solid lubricant” graphite, the rocks are loose and fractured with poor stability, especially the cataclastic breccia. Compared with the host rock, their structure and composition are strongly changed after being subjected to tectonic stress and hydrothermal alteration, and the mechanical properties will be significantly weakened. These are important intrinsic geological factors for the occurrence of jamming accidents.
- Geological structure: the trend of the reverse fault FT₂ (N20–30°E) intersects the tunnel’s strike (N7.6°E) obliquely at a small angle, which leads to a long section of the tunnel affected by the fault. The uneven distribution of the local ground stress field on the hanging wall and footwall of the fault leads to uneven deformation and failure of the left and right sides of the tunnel and the left upper part of the cave collapsed and deformed seriously.
- Ground stress: as shown in Table 1, the average unit weight of the overlying rock mass is approximately 28 kN/m³, and the tunnel in the TBM jamming section is buried at a depth of about 465 m, and then the maximum horizontal principal stress value (19.75 Mpa) or the vertical principal stress value (17.94 Mpa) is all higher than the gravity-induced stress value (13.02 Mpa). The orientation of the maximum horizontal principal stress is N82°E–N86°E, intersecting with the tunnel’s strike (N7.6°E) at a large angle, which is detrimental to the stability of the tunnel.

Fig. 14 The graphite carbon contents of rock samples



- TBM excavation: TBM excavation unloading leads to stress release and breaks the original equilibrium state of the rock mass. Therefore, TBM excavation is the external trigger factor for the occurrence of jamming accidents.

Therefore, the comprehensive effect of the above factors leads to collapse and large deformation of the weak rock in the fault zone as the main geological reason for the TBM jamming.

Engineering treatment measures and recommendations

Having identified the main geological cause of the TBM jamming at mileage 106+402.8, we filled and chemically consolidate the cavity on the left side of the tunnel to prevent the surrounding rock near the cavity from collapsing again (Wang et al. 2020). After clearing the collapsed rocks, the cavity port is supported by square pieces of wood or planks, the support structure is consolidated with reinforced chemical grouting material, and the cavity is quickly filled and sealed (Fig. 15a, b). We use the pneumatic pick to expand small pilot tunnels (1 m wide and 1.5 m high) from both

sides of the front and rear shield (Fig. 15c), and during the process of expanding excavation, square pieces of wood and I-beam are used to support the roof and sidepiece of the pilot tunnels in time to prevent falling rocks from hurting people and the pilot tunnels from collapsing (Fig. 15d).

In addition, since the continued excavation section is located on the hanging wall of the FT₂ fault and the rock is relatively weak, the following treatment measures are also suggested to prevent the recurrence of jamming accidents after releasing the TBM:

- To increase the reserved expansion gap between the shield and the surrounding rock, cushion blocks of 1 cm to 5 cm can be installed at the bottom of the cutter box, which makes the edge disc cutter move outward.
- To prevent the clay minerals from being softened and swelled when subjected to water and causing the cutter head to jam again, it is recommended to clean up the rock fragments in and around the cutter head in time.
- Chemical grouting and cement-based grouting methods are used alternately to consolidate the fractured surrounding rock in front of the tunnel face and above the front shield.



Fig. 15 Engineering treatment measures adopted for releasing TBM. **a** Supporting the collapsed cavity port with planks. **b** Chemical consolidation grouting. **c** Expanding excavation on both sides of the shield. **d** Supporting the pilot tunnels with square pieces of wood

Conclusions

To better understand the TBM jamming issues that occurred in our underground tunnel, we explored the microstructures, geochemistry, and mineralogical characteristics of the host and fault rocks in the FT₂ fault zone. We obtained evidence for the weakening of the mechanical characteristics of the fault rock. Based on the analysis of geological structure, ground stress, and rock mechanics parameters, the engineering geological reasons for the occurrence of the TBM jamming are derived, and corresponding engineering treatment measures and recommendations are proposed following local conditions. Our conclusions are as follows:

- (1) The fault rocks have typically cataclastic breccia and mylonite fabrics. Compared with the host rock, their structure and composition are strongly changed after being subjected to tectonic stress and hydrothermal alteration. Rich in clay minerals chlorite and “solid lubricant” graphite, the particle size is greatly decreased, and the cementation between the mineral particles is weakened, the rocks are loose and fractured with poor stability, and the mechanical properties significantly weakened.
- (2) The comprehensive effect of the geological characteristics of fault rock, geological structure, ground stress, and TBM excavation unloading leads to collapse and large deformation of the weak rock in the fault zone as the main geological reason for the TBM jamming.
- (3) After releasing the TBM by expanding the small pilot tunnels and chemical consolidation grouting, to prevent the recurrence of the jamming accident, it is also recommended to take measures to install cushion blocks at the bottom of the cutter box, clean up the rock fragments inside, and around the cutter and use advanced chemical grouting reinforcement.

Acknowledgements The authors would like to thank the editors and reviewers for their time and effort in reviewing and improving this paper.

Funding We would like to acknowledge the financial support from the Natural Science Foundation of China (Grant No. 52022053), the Natural Science Foundation of Shandong Province (Grant No. ZR201910270116), the Natural Science Foundation of Jiangsu Province (Grant No. BK20200227), and the China Postdoctoral Science Foundation (Grant No. 2019M662361).

Code availability No code was included in this paper.

Declarations

Ethics approval and consent for publication The paper follows scientific ethical standards. The authors are happy to provide consent for publication.

Conflict of interest The authors declare no competing interests.

References

- Abd Elmola A, Charpentier D, Buatier M, Lanari P, Monié P (2017) Textural-chemical changes and deformation conditions registered by phyllosilicates in a fault zone (Pic de Port Vieux thrust, Pyrenees). *Appl Clay Sci* 144:88–103
- Aydan Ö, Hasanpour R (2019) Estimation of ground pressures on a shielded TBM in tunneling through squeezing ground and its possibility of jamming. *Bull Eng Geol Env* 78:5237–5251
- Bayati M, Khademi Hamidi J (2017) A case study on TBM tunneling in fault zones and lessons learned from ground improvement. *Tunn Undergr Space Technol* 63:162–170
- Bejari H, Khademi Hamidi J (2018) A parametric study of two solutions for TBM jamming problem in squeezing ground conditions. *Int J Civ Eng Tech* 9:862–878
- Bilgin N (2016) An appraisal of TBM performances in Turkey in difficult ground conditions and some recommendations. *Tunn Undergr Space Technol* 57:265–276
- Bradbury KK, Davis CR, Shervais JW, Janecke SU, Evans JP (2015) Composition, alteration, and texture of fault-related rocks from SAFOD core and surface outcrop analogs: evidence for deformation processes and fluid-rock interactions. *Pure Appl Geophys* 172:1053–1078
- Cao SY, Neubauer F (2019) Graphitic material in fault zones: implications for fault strength and carbon cycle. *Earth Sci Rev* 194:109–124
- Chen JY, Yang XS, Ma SL, Spiers C (2013) Mass removal and clay mineral dehydration/rehydration in carbonate-rich surface exposures of the 2008 Wenchuan earthquake fault: geochemical evidence and implications for fault zone evolution and coseismic slip: mass removal and clay transformation. *J Geophys Res Solid Earth* 118
- Chen ZQ, He C, Yang WB, Guo WQ, Li Z, Xu GW (2020) Impacts of geological conditions on instability causes and mechanical behavior of large-scale tunnels: a case study from the Sichuan-Tibet highway, China. *Bull Eng Geol Env* 79:3667–3688
- Chester F, Evans J, Biegel R (1993) Internal structure and weakening mechanisms of the San Andreas Fault. *J Geophys Res* 98:771–786
- Craw D, Upton P (2014) Graphite reaction weakening of fault rocks, and uplift of the Annapurna Himal, central Nepal. *Geosphere* 10:720–731
- Crespo Feo E, Luque J, Barrenechea J, Rodas M (2005) Mechanical graphite transport in fault zones and the formation of graphite veins. *Mineralogical Magazine - MINER MAG* 69:463–470
- Duan QB, Yang XS, Ma SL, Chen JY, Chen JY (2016) Fluid–rock interactions in seismic faults: implications from the structures and mineralogical and geochemical compositions of drilling cores from the rupture of the 2008 Wenchuan earthquake, China. *Tectonophysics* 666:260–280
- Farrokh E, Rostami J (2009) Effect of adverse geological condition on TBM operation in Ghomroud tunnel conveyance project. *Tunn Undergr Space Technol* 24:436–446
- Haertel M, Herwegh M, Pettke T (2013) Titanium-in-quartz thermometry on synkinematic quartz veins in a retrograde crustal-scale normal fault zone. *Tectonophysics* 608:468–481
- Haines SH, van der Pluijm BA (2012) Patterns of mineral transformations in clay gouge, with examples from low-angle normal fault rocks in the western USA. *J Struct Geol* 43:2–32
- Hasanpour R, Rostami J, Schmitt J, Ozelcik Y, Sohrabian B (2020) Prediction of TBM jamming risk in squeezing grounds using Bayesian and artificial neural networks. *Journal of Rock Mechanics and Geotechnical Engineering* 12:21–31

- Hirono T, Fujimoto K, Yokoyama T, Hamada Y, Tanikawa W, Tadao O, Mishima T, Tanimizu M, Lin WR, Soh W, Song SR (2008) Clay mineral reactions caused by frictional heating during an earthquake: an example from the Taiwan Chelungpu fault. *Geophys Res Lett* 35:L16303
- Holdsworth RE, van Diggelen EWE, Spiers CJ, de Bresser JHP, Walker RJ, Bowen L (2011) Fault rocks from the SAFOD core samples: implications for weakening at shallow depths along the San Andreas Fault, California. *J Struct Geol* 33:132–144
- Isaacs A, Evans J, Song SR, Kolesar P (2007) Structural, mineralogical, and geochemical characterization of the Chelungpu Thrust Fault, Taiwan. *Terrestrial Atmospheric and Oceanic Sciences - TERR ATMOS OCEAN SCI* 18
- Janssen C, Kanitpanyacharoen W, Wenk HR, Wirth R, Morales L, Rybacki E, Kienast M, Dresen G (2012) Clay fabrics in SAFOD core samples. *J Struct Geol* 43:118–127
- Janssen C, Wirth R, Wenk HR, Morales L, Naumann R, Kienast M, Song SR, Dresen G (2014) Faulting processes in active faults – evidences from TCDP and SAFOD drill core samples. *J Struct Geol* 65:100–116
- Kuo LW, Li HB, A.F. Smith S, Toro DG, Suppe J, Song SR, Nielsen S, Sheu HS, Si JL (2014) Gouge graphitization and dynamic fault weakening during the 2008 Mw 7.9 Wenchuan earthquake. *Geol* 42:47–50
- Kuo LW, Song SR, Yeh EC, Chen HF (2009) Clay mineral anomalies in the fault zone of the Chelungpu Fault, Taiwan, and their implications. *Geophys Res Lett* 36
- Li HB, Wang H, Xu ZQ, Si JL, Pei JL, Li TF, Huang Y, Song SR, Kuo LW, Sun ZM, Chevalier ML, Liu DL (2013) Characteristics of the fault-related rocks, fault zones and the principal slip zone in the Wenchuan Earthquake Fault Scientific Drilling Project Hole-1 (WFSD-1). *Tectonophysics* 584:23–42
- Li SC, Xu ZH, Huang X, Lin P, Zhao XC, Zhang QS, Yang L, Zhang X, Sun HF, Pan DD (2018) Classification, geological identification, hazard mode and typical case studies of hazard-causing structures for water and mud inrush in tunnels. *J Rock Mec Eng* 37:1041–1069 (in Chinese)
- Liao CZ, Zhang YQ, Wen CS (2007) Structural styles of the eastern boundary zone of the Ordos Basin and its regional tectonic significance. *Acta Geologica Sinica*:466–474 (in Chinese)
- Lin A (2005) Meso and microstructural analysis of coseismic shear zone of the 1999 MW 7.6 Chi-Chi Earthquake. *Taiwan Bulletin of the Seismological Society of America - BULL SEISMOL SOC AMER* 95:486–501
- Lin DM, Yuan RM, Shang YJ, Bao WX, Wang KY, Zhang ZJ, Li K, He WT (2017) Deformation and failure of a tunnel in the restraining bend of a strike-slip fault zone: an example from Hengshan Mountain, Shanxi Province, China. *Bull Eng Geol Env* 76:263–274
- Liu QS, Liu H, Huang X, Pan YC, Luo CY, Sang HM (2019) Inverse analysis approach to identify the loads on the external TBM shield surface and its application. *Rock Mech Rock Eng* 52:3241–3260
- Lyu M, Cao SY, Neubauer F, Li JY, Cheng XM (2020) Deformation fabrics and strain localization mechanisms in graphitic carbon-bearing rocks from the Ailaoshan-Red River strike-slip fault zone. *J Struct Geol* 140:104150
- Matsuda T, Arai T, Ikeda R, Omura K, Kobayashi K, Sano H, Sawaguchi T, Tanaka H, Tomita T, Tomida N, Hirano S, Ymazaki A (2001) Examination of mineral assemblage and chemical composition in the fracture zone of the Nojima Fault at a depth of 1140 m: analyses of the Hirabayashi NIED drill cores. *Island Arc* 10:422–429
- Matsuda T, Omura K, Ikeda R, Arai T, Kobayashi K, Shimada K, Tanaka H, Tomita T, Hirano S (2004) Fracture-zone conditions on a recently active fault: insights from mineralogical and geochemical analyses of the Hirabayashi NIED drill core on the Nojima fault, southwest Japan, which ruptured in the 1995 Kobe earthquake. *Tectonophysics* 378:143–163
- Moore DE, Lockner DA (2008) Talc friction in the temperature range 25°–400 °C: relevance for Fault-Zone Weakening. *Tectonophysics* 449:120–132
- Nakamura Y, Oohashi K, Toyoshima T, Satish-Kumar M, Akai J (2015) Strain-induced amorphization of graphite in fault zones of the Hidaka metamorphic belt, Hokkaido, Japan. *J Struct Geol* 72:142–161
- Niwa M, Shimada K, Ishimaru T, Tanaka Y (2019) Identification of capable faults using fault rock geochemical signatures: a case study from offset granitic bedrock on the Tsuruga Peninsula, central Japan. *Engineering Geology* 260:105235
- Numelin T, Marone C, Kirby E (2007) Frictional properties of natural fault gouge from a low-angle normal fault, Panamit Valley, California. *Tectonics* 26
- Oohashi K, Hirose T, Kobayashi K, Shimamoto T (2012) The occurrence of graphite-bearing fault rocks in the Atotsugawa fault system, Japan: origins and implications for fault creep. *J Struct Geol* 38:39–50
- Oohashi K, Hirose T, Shimamoto T (2011) Shear-induced graphitization of carbonaceous materials during seismic fault motion: experiments and possible implications for fault mechanics. *J Struct Geol* 33:1122–1134
- Peng JB, Ma RY, Shao TQ (2004) Basic relation between structural geology and engineering geology. *Earth Science Frontiers*:535–549 (in Chinese)
- Schleicher A, Sutherland, Townend, Toy V, Van der Pluijm B (2015) Clay mineral formation and fabric development in the DFDP-1B borehole, central Alpine Fault, New Zealand New Zealand. *J Geol Geophys* 58
- Schleicher A, Tourscher S, Van der Pluijm B, Warr L (2009) Constraints on m-ineralization, fluid-rock interaction, and mass transfer during faulting at 2–3 km depth from the SAFOD drill hole. *J Geophys Res* 114
- Scholz C (1987) Wear and gouge formation in brittle faulting. *Geology* 15:493–495
- Shang YJ, Xue JH, Wang SJ, Yang ZF, Yang J (2004) A case history of tunnel boring machine jamming in an inter-layer shear zone at the Yellow River Diversion Project in China. *Eng Geol* 71:199–211
- Sun Y, Xu SJ, Liu DL, Lin AM, Lu JJ (1998) An introduction of tectono-geochemistry in fault zones. Science Press (in Chinese)
- Tanaka H, Fujimoto K, Ohtani T, Ito H (2001) Structural and chemical characterization of shear zones in the freshly activated Nojima fault, Awaji Island, southwest Japan. *J Geophys Res Solid Earth* 106:8789–8810
- Trincal V, Charpentier D, Buatier MD, Grobety B, Lacroix B, Labaume P, Sizun J-P (2014) Quantification of mass transfers and mineralogical transformations in a thrust fault (Monte Perdido thrust unit, southern Pyrenees, Spain). *Mar Pet Geol* 55:160–175
- Wang Q, Xin X, Jiang B, Sun HB, Xiao YC, Bian WH, Li LN (2020) Comparative experimental study on mechanical mechanism of combined arches in large section tunnels. *Tunn Undergr Space Technol* 99: 103386
- Warr L, Cox S (2001) Clay mineral transformations and weakening mechanisms along the Alpine Fault, New Zealand. *Geol Soc London Spec Publ* 186:85–101
- Williams JN, Toy VG, Smith SAF, Boulton C (2017) Fracturing, fluid-rock interaction and mineralisation during the seismic cycle along the Alpine Fault. *J Struct Geol* 103:151–166
- Xu ZH, Lin P, Xing HL, Wang J (2020b) Mathematical modelling of cumulative erosion ratio for suffusion in soils. *P I Civil Eng-Geotec* 174: 241–251
- Xu ZH, Liu FM, Lin P, Shao RQ, Shi XS (2021c) Non-destructive in-situ fast identification of adverse geology in tunnels based on

- anomalies analysis of element content. *Tunn Undergr Space Technol* 118:104146
- Xu ZH, Ma W, Lin P, Shi H, Pan DD, Liu TH (2021a) Deep learning of rock images for intelligent lithology identification. *Comput Geosci-UK* 154:104799
- Xu ZH, Shi H, Lin P, Liu TH (2021b) Integrated lithology identification based on images and elemental data from rocks. *J Petrol Sci Eng* 205:108853
- Xu ZH, Wang WY, Lin P, Nie LC, Wu J, Li ZM (2020a) Hard-rock TBM jamming subject to adverse geological conditions: influencing factor, hazard mode and a case study of Gaoligongshan Tunnel. *Tunn Undergr Space Technol* :103683
- Xue YG, Kong FM, Qiu DH, Su MX, Zhao Y, Zhang K (2020) The classifications of water and mud/rock inrush hazard: a review and update. *Bull Eng Geol Env* 80:1907–1925
- Zhang JZ, Zhou XP (2017) Time-dependent jamming mechanism for Single-Shield TBM tunneling in squeezing rock. *Tunn Undergr Space Technol* 69:209–222
- Zhang JQ, Li SC, Zhang QS, Zhang X, Li P, Wang DM, Weng XJ (2019) Mud inrush flow mechanisms: a case study in a water-rich fault tunnel. *Bull Eng Geol Env* 78:6267–6283
- Zhang N, Shen JS, Zhou A, Arulrajah A (2018) Tunneling induced geohazards in mylonitic rock faults with rich groundwater: a case study in Guangzhou. *Tunn Undergr Space Technol* 74:262–272